Computer models for studying interventions used in treating refractory pulmonary hypertension

Seong Woo Han BA[1], Charles Puelz PhD[2], Craig G. Rusin PhD[2],
Dan J. Penny MD, PhD, MHA[2], Ryan Coleman MD[2], and Charles S. Peskin PhD[1]

[1]Courant Institute of Mathematical Sciences, New York University
[2]Department of Pediatrics-Cardiology, Baylor College of Medicine

January 19, 2021

Abstract

This paper describes computer models for three palliations used in treating refractory pulmonary hypertension. These procedures effectively create an atrial septal defect, a ventricular septal defect, or a patent ductus arteriosus, also known as a Potts shunt. The aim in all three cases is to generate a right-to-left shunt, allowing for either pressure or volume unloading of the right side of the heart in the setting of right ventricular failure, while allowing for maintenance of cardiac output. However, these shunts are created at the expense of introducing de-oxygenated blood into the systemic circulation, thereby lowering the systemic arterial oxygen saturation. The models developed in this paper are based on compartmental descriptions of human hemodynamics and oxygen transport. An important parameter included in our models is the cross-sectional area of the surgically created defect. Numerical simulations are performed to compare different interventions and various shunt sizes and to assess their impact on hemodynamic variables and oxygen saturations.

1 Introduction

Pulmonary hypertension refers to a spectrum of cardiovascular and/or pulmonary diseases that involve elevations in a person's pulmonary vascular resistance (PVR). Over time, this elevated PVR causes pathologic remodeling of the right ventricle and the pulmonary vasculature, ultimately resulting in right ventricular failure and death. In this paper, our focus is on interventions for refractory pulmonary hypertension, which corresponds to disease that is unresponsive to standard medical treatments [5, 10]. Even with aggressive pharmacotherapy, patients often will ultimately require either lung transplantation or palliative surgical or catheter-based procedures, with the goals of either approach being aimed at providing relief to the ailing right ventricle and extending the patient's life for an unknown period of time.

Palliative shunts used in the setting of a failing right ventricle due to elevated PVR can be classified into two main categories: (1) pre-tricuspid shunts, meaning the shunt occurs prior to blood crossing the tricuspid valve, which is what occurs in the setting of an atrial septal defect (ASD), and (2) post-tricuspid shunts, meaning the shunt occurs after the blood passes the tricuspid valve, which are where the ventricular septal defect (VSD) and patent ductus arteriosis (PDA)/Potts shunt occur. This classification scheme is important, as pre-tricuspid shunts are viewed as volume-unloading shunts for the right ventricle, meaning they can unload excess volume from a failing

right ventricle, but do not directly affect the pressure the right ventricle has to pump against. Post-tricuspid shunts, on the other hand, are pressure-unloading shunts, meaning they provide a lower-resistance pathway for blood to traverse, decreasing the resistance the failing right ventricle has to pump against. Pressure-unloading shunts are often preferred, as it is the pressure load the right ventricle has to pump against that results in its failure and patient demise. However, because these shunts, regardless of location, allow for right-to-left shunting, they result in a decrease in systemic oxygen saturations of varying degrees and severity. Shunt effectiveness is determined not only by location of the shunt, but by the size of the shunt as well. Small septal defects may quickly become restrictive over time, reducing their effectiveness at either pressure- or volume-unloading the right ventricle. The same is true for narrow shunts (either PDA/Potts shunt), particularly as their length increases.

The effects of various shunts on pressures, flows, and oxygen saturations are often not clear in practice. Furthermore, shunt flows are highly sensitive to shunt size, a parameter that can be varied within the modeling framework developed herein. The goal of this paper is to use computational models to study the impact of several possible shunts, used for treating refractory pulmonary hypertension, on important hemodynamic variables and oxygen saturations. The three shunts considered here are either within the (1) atrial septum, (2) ventricular septum, or (3) between the main pulmonary artery and aorta [9, 2]. We refer to these surgically created defects respectively by the following names: (1) an atrial septal defect (ASD), (2) a ventricular septal defect (VSD), or (3) a Potts shunt. For each intervention, we develop and apply computational models to study both the benefit in terms of reduced pulmonary artery pressure and also the detriment in terms of systemic arterial oxygen desaturation, as functions of the cross-sectional area of the shunt.

The complexities associated with pulmonary hypertension have motivated the use of computational models for "non-invasively" studying disease progression, diagnosis, and the performance of possible treatments. We recall several important contributions of physics-based models for pulmonary hypertension. Delhass et al. constructed compartmental models for two possible interventions considered in this paper, the ASD and the Potts shunt [4]. Our paper extends their results to a comparison of the ASD and Potts shunt with the VSD. Acosta et al. used vessel network models of pulmonary hypertension to derive early diagnostic indicators of disease [1]. Qureshi et al. also used vessel network models coupled to fractal descriptions of the small vessel networks to study several classes of pulmonary hypertension [16]. There have also been modeling efforts to understand the impact of pulmonary hypertension on remodeling of heart tissue. Raush et al. constructed three-dimensional solid mechanics models of the ventricular chambers that were coupled to a mathematical description of tissue remodeling under the high pressure loads associated with hypertension [17].

The rest of this paper is organized as follows. Section 2 describes the mathematical models for blood flow and oxygen transport and the numerical methods used to approximate the resulting equations. That section also includes a discussion of parameter selection and the shunt model derived from the Gorlin equation. Section 3 details results from our models for each of the three possible surgical interventions. Our models are used to study the dependence of several important hemodynamic variables on shunt size, and we also investigate the time-dependent details of the shunt flow waveform. Conclusions are provided in section 5.

2   Circulation models and numerical methods

In this section, we present the models used in this work and the numerical methods by which the model equations are solved. The following subsections describe a hemodynamic model, a cardiac

chamber model that specifies the time-varying compliance of each heart chamber in the hemodynamic model, a shunt model based on the Gorlin equation that makes it possible to include shunts of specified cross-sectional area in the hemodynamic model, and finally an oxygen transport model that calculates oxygen saturations throughout the model circulation based on the flows obtained from the hemodynamic model.

2.1 Hemodynamic model

The circulation is represented by a collection of compartments corresponding to compliance chambers. These chambers are connected by resistors that are equipped with valves [15]. We use the following compliance relation for each of the N compliance chambers, numbered $i = 1, 2, ..., N$:

$$V_i = (V_\mathrm{d})_i + C_i P_i, \quad i = 1, ..., N. \tag{1}$$

The parameter C_i is the compliance of chamber i, which is assumed to be constant for arteries and veins but time-varying for the heart chambers. The variable V_i is the volume of compliance chamber i, the variable P_i is the pressure of that chamber, and the parameter $(V_\mathrm{d})_i$ is the dead volume, that is, the volume of the chamber when the pressure is zero. We assume the flow from chamber i to chamber j is governed by a pressure-flow relationship of the following form:

$$Q_{ij} = \frac{S_{ij}}{R_{ij}}(P_i - P_j) = S_{ij} \, G_{ij} \, (P_i - P_j), \quad i, j = 1, ..., N, \tag{2}$$

where

$$S_{ij} = \begin{cases} 1, & P_i > P_j, \\ 0, & P_i \le P_j. \end{cases} \tag{3}$$

Equation (2) describes the flow through a resistance that is equipped with a valve. The conductance G_{ij} is the reciprocal of the resistance R_{ij}. Conductance is convenient because it can be set equal to zero to represent the absence of a connection between two chambers. The variable S_{ij}, which is determined by P_i and P_j according to equation (3), denotes the state of the valve, with $S_{ij} = 1$ when the valve is open, and $S_{ij} = 0$ when the valve is closed. (Note that the words "open" and "closed" have the opposite meaning here from their use in electricity, where a closed switch is conducting and an open switch is non-conducting.)

Equipping *every* connection with a valve does not involve any loss of generality. Between any pair of chambers i and j, our framework allows for *two* connections of the type described above, one with a valve that allows flow only from i to j, and another with a valve that allows flow only from j to i. To model a situation in which there is no valve in a connection between chambers i and j, we need only set G_{ij} equal to G_{ji}. To model a leaky valve we may set G_{ij} and G_{ji} to positive but unequal values. Lastly, to model the situation in which there is no connection at all between chambers i and j, we set $G_{ij} = G_{ji} = 0$. Thus, our framework allows for a great variety of connection types and patterns merely by specifying the (non-symmetric) N by N matrix G.

Upon differentiating equation (1) with respect to time and using the principle that the rate of change of volume is equal to inflow minus outflow, together with equation (2), one obtains the

following system of ordinary differential equations for the pressures as functions of time:

$$\frac{d}{dt}(C_i P_i) = \sum_{j=1}^{N}(S_{ji}G_{ji}(P_j - P_i) - S_{ij}G_{ij}(P_i - P_j))$$

$$= \sum_{j=1}^{N}(S_{ij}G_{ij} + S_{ji}G_{ji})(P_j - P_i). \tag{4}$$

We assume here that all of the dead volumes are constant but allow for the possibility that some of the compliances, specifically those of the heart chambers, are functions of time. How these compliances are specified will be described in subsection 2.2. Equation (4) will be modified later to include shunt flows modeled by the Gorlin equation; see subsection 2.3.

Our numerical scheme for equation (4) is the backward Euler method:

$$\frac{C_i^n P_i^n - C_i^{n-1}P_i^{n-1}}{\Delta t} = \sum_{j=1}^{N}(S_{ij}^n G_{ij}^n + S_{ji}^n G_{ji}^n)(P_j^n - P_i^n). \tag{5}$$

This is a system of equations for the unknown pressures at time step n. It is a nonlinear system, because S_{ij} is a function of P_i and P_j, see equation (3). The reason for using the backward Euler method here is its unconditional stability. If two compliance chambers are connected by a very large conductance (that is, by a very small resistance), their pressures will equilibrate on a very fast time scale, and we do not want to be required to use a small enough time step to resolve the details of that rapid equilibration. This situation actually arises in the circulation whenever there are two chambers with an open heart valve between them, since an open valve (at least when it is non-stenotic) has a very high conductance.

The procedure that we use to solve the nonlinear system (5) is based on the following observation: given the valve states, equation (5) is reduces to a linear system that is easy to solve for the pressures. Also, given the pressures, it is easy to evaluate the valve states from equation (3). Thus, the procedure starts with a guess for the valve states (a good guess is the valve states that were found on the previous time step), solves equation (5) for the pressures, resets the valve states according to the pressures via equation (3), and so on. The process stops when the valve states (and therefore the pressures) stop changing, and in practice this happens very quickly. On most time steps, the initial guess, that the valves states are the same as they were at the previous time step, turns out to be correct. When the valve states stop changing, the problem stated in equation (5) is actually solved (except, of course, for round-off error), not merely solved to within some tolerance. This is because the valve states are discrete.

For further discussion of the methodology described here, see [7]. As in that reference, our models use six compliance chambers corresponding to the left and right ventricles and the systemic and pulmonary arteries and veins. We do not separately model the atria, but instead treat each atrium as part of the venous system to which it is connected, and moreover we do not take into account the time dependence of the atrial compliances. The ventricular compliances are, of course, time dependent in our model, but not in the same way as in [7], see section 2.2.

In order to model severe pulmonary hypertension, the pulmonary resistance is taken to be 1.5 times greater than the systemic resistance [19]. This is very different from the normal case in which the pulmonary resistance is approximately 10 times *smaller* than the systemic resistance [8, 13, 25]. A possible consequence of pulmonary hypertension is right-heart hypertrophy, making the normally thin-walled right ventricle into a chamber that more closely resembles the normal left ventricle [20, 14, 3]. To model this, we use typical left-ventricular parameters for both ventricles;

4

Parameters	Resistance (R)	Dead Volume (V_d)	Compliance (C)
Units	mmHg/(L/min)	L	L/mmHg
S	17.5	-	-
P	26.25	-	-
Mi	0.01	-	-
Ao	0.01	-	-
Tr	0.01	-	-
Pu	0.01	-	-
SA	-	0.825	0.00175
PA	-	0.0382	0.00175
SV	-	0	1.75
PV	-	0	0.08

Table 1: Parameters for the circulation model. Pulmonary resistance is chosen to be 1.5 times greater than the systemic resistance to simulate refractory pulmonary hypertension. Abbreviations: S, systemic organs; P, lungs; Mi, mitral valve; Ao, aortic valve; Tr, tricuspid valve; Pu, pulmonic valve; SA, systemic arteries; PA, pulmonary arteries; SV, systemic veins; PV, pulmonary veins.

see the next section. Another consequence of pulmonary hypertension is right heart failure that leads to increased blood volume [23]. Accordingly, we use a total blood volume of 8.68 L, instead of a normal blood volume, which would be about 5 L. This change is needed to elevate the systemic venous pressure sufficiently to fill the hypertrophied right heart and produce a viable cardiac output. With these exceptions, we are using the same parameters as in [7]. The hemodynamic parameters used in the present model, other than the cardiac chamber parameters, are stated in Table 1.

2.2 Cardiac chamber model

This section details the time-varying elastance model used for the left and right ventricles, adapted from [12]. Note that the elastance, denoted by E, is the reciprocal of the compliance C. For a cardiac chamber, the elastance, and therefore the compliance, is a given function of time. In this work, we use the same elastance function $E(t)$, with the same parameters, for the left and right ventricles. This choice is reasonable because the large right-sided pressures associated with pulmonary hypertension lead to remodeling and thickening of the right ventricular wall [6]. In severe pulmonary hypertension, these changes result in a right ventricular pressure/volume characteristics similar to that of the left ventricle [21]. Maximum and minimum ventricular elastances are denoted E_max and E_min. E_max is the end-systolic elastance and E_min is the end-diastolic elastance. The functional form of the elastance $E(t)$ is given during the time interval $[0, T]$ as follows:

$$E(t) = k \left(\frac{g_1(t)}{1 + g_1(t)} \right) \left(\frac{1}{1 + g_2(t)} - \frac{1}{1 + g_2(T)} \right) + E_\mathrm{min}, \tag{6}$$

where

$$g_1(t) = \left(\frac{t}{\tau_1} \right)^{m_1}, \quad g_2(t) = \left(\frac{t}{\tau_2} \right)^{m_2}. \tag{7}$$

Here T is the period of the heartbeat. Note that equation (6) makes $E(0) = E(T)$. (We have made a slight modification of the formula used in [12] to ensure this.) Outside of the interval $[0, T]$, we

Parameters	Symbol	Units	Left Ventricle	Right Ventricle
Minimal elastance	$E_{\min}$	mmHg/L	0.08×10^3	0.08×10^3
Maximal elastance	$E_{\max}$	mmHg/L	30.00×10^3	30.00×10^3
Contraction exponent	m_1	-	1.32	1.32
Relaxation exponent	m_2	-	27.4	27.4
Systolic time constant	τ_1	min	0.269T	0.269T
Diastolic time constant	τ_2	min	0.452T	0.452T
Dead Volume	V_d	L	0.010	0.010
Period of heartbeat	T	min	0.0125	0.0125

Table 2: Parameters for the time varying compliances in the heart model.

define $E(t)$ as a periodic function with period T, so that $E(t) = E(t + T)$ for all t. The parameter k is chosen so that the maximum value of $E(t)$ is $E_{\max}$. The formula for k to achieve this is

$$k = \frac{E_{\max} - E_{\min}}{\max_{t \in [0,T]}[(\frac{g_1(t)}{1+g_1(t)})(\frac{1}{1+g_2(t)} - \frac{1}{1+g_2(T)})]} \tag{8}$$

The maximum in the denominator of the formula for k is computed by evaluating the expression that needs to be maximized at a collection of equally spaced points within the interval $[0, T]$, and then choosing the largest of the values of that expression that are found. Although this procedure does not yield the exact maximum value, it comes close enough for practical purposes, especially since the goal is to find the maximum value, rather than the time at which it occurs. Parameter values used for the heart chambers are provided in Table 2. The constant τ_1 controls the timescale of contraction, τ_2 controls the duration of systole, and m_1 and m_2 govern the speed of contraction and relaxation respectively. Note that τ and m are estimated from previously employed values [22], and the values for $E_{\min}$ and $E_{\max}$ are similar to those used by [11].

2.3 Shunt model

The Gorlin equation is used to calculate flows through surgically created shunts (ASD, VSD, or Potts shunt) in our model [18]. This allows us to specify the cross-sectional area of the connection that the surgeon creates, and to study how the shunt size affects hemodynamic variables and the transport of oxygen.

To derive the shunt model, consider two chambers, denoted by the indices 1 and 2, separated by a wall with a hole in it that corresponds to the shunt. Let A_0 be the cross-sectional area of the hole. We assume that the velocity of the blood as it goes through the hole is much larger than the velocity in the two chambers, so that we may consider the fluid in each of the two chambers as if it were at rest. Let Q denote the volume of blood flow per unit time through the hole, with the direction from chamber 1 to chamber 2 considered positive. Then, the spatially averaged velocity of blood flow in the hole itself is given by

$$v = Q/A_0. \tag{9}$$

Let P_1 and P_2 be the pressures in the two chambers, and let P_0 be the pressure within the hole. Suppose, for example, that $Q > 0$. By Bernoulli's equation in the upstream chamber up to the hole itself, one has

$$P_0 = P_1 - \frac{1}{2}\rho v^2 = P_1 - \frac{\rho}{2A_0^2}Q^2. \tag{10}$$

In the region downstream of the hole, Bernoulli's equation does not apply because the flow there is dominated by turbulent eddies that dissipate energy. The result is that the pressure is relatively constant in the downstream region, in particular that $P_2 = P_0$. It follows that

$$P_1 - P_2 = \frac{\rho}{2A_0^2}Q^2, \quad Q > 0. \tag{11}$$

By the same reasoning, for flow in the other direction

$$P_2 - P_1 = \frac{\rho}{2A_0^2}Q^2, \quad Q < 0. \tag{12}$$

Equations (11) and (12) can be combined as follows:

$$P_1 - P_2 = \frac{\rho}{2A_0^2}|Q|Q, \tag{13}$$

This shows that the hydraulic resistance of the hole is given by

$$R_{\text{shunt}} = \frac{\rho}{2A_0^2}|Q|. \tag{14}$$

Note that the above formula for R_{shunt} is independent of viscosity. In reality, there is a very small viscous resistance as well, so we modify the above formula to read

$$R_{\text{shunt}} = R_{\text{visc}} + \frac{\rho}{2A_0^2}|Q|. \tag{15}$$

In most situations R_{visc} is negligible, but we should include it to prevent R_{shunt} from being zero, which would otherwise happen in principle every time that Q changes sign. Since R_{visc} is included only for this reason, we choose the very small value $R_{\text{visc}} = 0.1$ mmHg/(L/min). Evaluating the conductance of the hole from equation (15), one obtains

$$G_{\text{shunt}} = \frac{1}{R_{\text{visc}} + \frac{\rho}{2A_0^2}|Q|} \tag{16}$$

In making use of equation (16), one must be careful about units. In this paper, we use what may be called physiological units, in which volume is measured in liters, pressure in mmHg, and time in minutes. The constants A_0 and ρ need to be expressed in these units. The use of liters for volume implies that our unit of length is the decimeter (dm), which is equal to 10 cm. Thus, A_0 needs to be expressed internally in terms of dm^2, although in the presentation of our results, we use cm^2 since these units have more meaning to the reader. To express density in physiological units, one needs the units of mass. The units of force are mmHg $\cdot$ dm^2, and the units of acceleration are dm/min^2, so the units of mass are mmHg $\cdot$ dm $\cdot$ min^2. Dividing this by dm^3, one obtains the units of density as mmHg $\cdot$ (min/dm)^2. After taking units carefully into account in this way, the density in physiological units is

$$\rho = 0.00002084167 \cdot \frac{\text{mmHg} \cdot \text{min}^2}{\text{dm}^2}. \tag{17}$$

Another complication in the use of equation (16) is that the shunt conductance G_{shunt} is flow-dependent. A simple idea here would be to use the shunt flow on the previous time step to set the shunt conductance for the present time step, but instead of this, we use a fixed-point iteration, with the shunt flow on the previous time step as the initial guess. At each step of the fixed-point

iteration, equation (16) is used to set the shunt conductance based on the latest guess for the shunt flow. Then, the shunt conductance is inserted into the appropriate two places in the conductance matrix G (one entry for each flow direction, since there is no valve involved in the shunt). Finally, all of the pressures and flows for the circulation are computed, including the shunt flow. The benefit of doing the fixed-point iteration can be seen in Figure 1 since it removes the numerical oscillations seen in the blood flow waveform. In practice, 10 fixed-point iterations are used for each time step, and this achieves good enough agreement between the flow that is used to set the shunt conductance and the flow that is calculated on the basis of that shunt conductance.
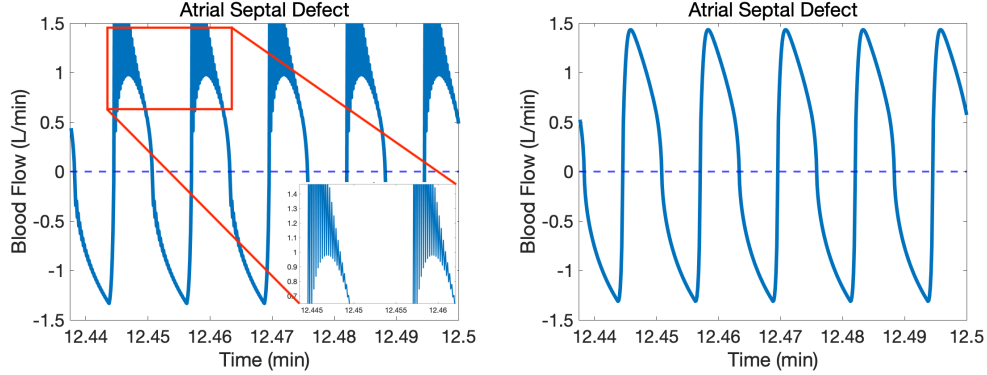

Figure 1: A comparison of shunt flow results with the ASD model, obtained with and without fixed-point iterations. The shunt area is 1 cm^2. The left panel shows flow computed without the fixed-point iteration. The right panel shows flow computed with the fixed-point iteration.

2.4 Oxygen transport model

An important consequence of the surgical interventions considered in this paper is the mixing of oxygenated and doxygenated blood. Our approach to the modeling of oxygen transport follows Tu and Peskin [24]. Time-varying oxygen concentrations for each compliance chamber are described by the following system of differential equations:

$$\frac{d}{dt}([O_2]_i V_i) = \sum_{\substack{j=1 \\ j \neq i}}^{N} ([O_2]_j Q_{ji} - [O_2]_i Q_{ij} + M_{ji}). \tag{18}$$

The variable $[O_2]_i$ is the oxygen concentration in compliance chamber i, the variable Q_{ji} is the blood flow from j to i, and the parameter M_{ji} is the rate at which oxygen is added to the stream of blood that is flowing from chamber j to chamber i. Note that M_{ji} is positive if oxygen is being added to the blood stream, and negative if oxygen is being removed. The correctness of equation (18) relies on the fact that all of the flows that appear in it are positive or zero. This is a benefit of our formulation in which every connection is equipped with a valve, as described above in section 2.1. These equations describe conservation of oxygen during transport between chambers as well as metabolic consumption of oxygen within systemic organs and replenishment of oxygen within the lungs. After computing the flows at time step n, those flow values are used to numerically update the oxygen concentrations from time step $n-1$ to n as follows:

$$\frac{[O_2]_i^n V_i^n - [O_2]_i^{n-1} V_i^{n-1}}{\Delta t} = \sum_{\substack{j=1 \\ j \neq i}}^{N} ([O_2]_j^{n-1} Q_{ji}^n - [O_2]_i^{n-1} Q_{ij}^n + M_{ji}). \tag{19}$$

8

Note that this is the forward Euler method insofar as the oxygen concentrations are concerned, although it differs from the forward Euler method by using the flows at time step n. The manner in which M is determined for use in these equations is described below.

We use the millimole (mmol) as the unit for the amount of oxygen. It then follows from our other choices of units that the units of oxygen concentration are mmol/L and the units of the rate of oxygen consumption by the body are mmol/min. A standard concentration of hemoglobin in blood is 2.5 mmol/L, and since each hemoglobin molecule can carry four oxygen molecules, the oxygen concentration when hemoglobin is fully saturated is 10 mmol/L.

There are only two places in our model where the variable M that appears in equation (18) is nonzero. One of these is in the connection from the pulmonary arteries (pa) to the pulmonary veins (pv). We assume that $M_{\mathrm{pa,pv}}$ is such that the stream of blood flowing from the pulmonary arteries to the pulmonary veins becomes fully saturated with oxygen during its passage through the pulmonary capillaries. This gives the equation

$$M_{\mathrm{pa,pv}} = (10 \text{ mmol/L} - [O_2]_{\mathrm{pa}}) \, Q_{\mathrm{pa,pv}}. \tag{20}$$

Equation (20) is used to set $M_{\mathrm{pa,pv}}$ at every time step. Note that this is *not* the same as setting $[O_2]_{\mathrm{pv}} = 10$ mmol/L. The reason for this is that there may be other streams of blood entering the pulmonary venous compartment besides the one coming from the pulmonary arteries. In particular, since we regard the left atrium as being part of the pulmonary venous compartment, this will be the case when we are simulating a surgically created atrial septal defect.

The other nonzero value of M in our model is $M_{\mathrm{sa,sv}}$, which is negative, since it represents oxygen consumption by the tissues. This oxygen is extracted from the stream of blood that flows from the systemic arteries (sa) to the systemic veins (sv). In the simulations reported here, we keep $M_{\mathrm{sa,sv}}$ constant, and we calculate its value by noting that a normal cardiac output is 5.6 L/min and a normal amount of oxygen extraction by the systemic tissue is 30%. These values result in the following:

$$-M_{\mathrm{sa,sv}} = 0.3 \cdot (10 \text{ mmol/L}) \cdot (5.6 \text{ L/min}) = 16.8 \text{ mmol/min} \tag{21}$$

The initial value for the oxygen concentration is set to 10 mmol/L in all compartments. Simulations are run until all hemodynamic variables and oxygen concentrations have reached a periodic steady state. The values reported in the following section are averages over the last ten of the computed cardiac cycles.

3 Results and discussion

In this section, we examine the simulated effects for each of the three interventions on several hemodynamic variables. First, we investigate changes in pressure and oxygen saturation in the systemic and pulmonary arteries as the shunt size is varied. Second, we examine shunt flow direction to determine whether the shunt is indeed right-to-left, as anticipated, or is perhaps bidirectional. In these simulations, 100 time steps are used for each cardiac cycle. The heart rate is 80 beats/minute, and each computer experiment is run for 12.5 minutes of simulated time, thus covering 1,000 simulated heartbeats. This duration is sufficient for the simulation to achieve a periodic steady state for all variables in all cases. When we report a single value for any quantity as the result of a simulation, it is the average of that quantity over the last 5 cardiac cycles of that simulation.

3.1 Pressures and oxygen saturations

First, we consider the pressures and oxygen saturations for each intervention. Figure 2 shows the systemic and pulmonary arterial blood pressures (mean values) as functions of the shunt area. Results for the atrial septal defect (ASD) are in the left panel, results for the ventricular septal defect (VSD) are in the middle panel, and results for the Potts shunt are in the right panel. The ASD results show that this intervention is not successful in lowering the pulmonary arterial pressure, which is perhaps consistent with the fact that an ASD is a volume-unloading shunt. The insets in the figure confirm that there is actually a very small effect, but it is certainly not one that would be therapeutic. The VSD intervention lowers the mean pulmonary artery pressure from about 105 mmHg to about 85 mmHg, which could be beneficial. This result is achieved by a shunt with cross-sectional area equal to 0.6 cm^2. It is interesting to note that beyond this value for the area, the pulmonary arterial pressure slightly increases as the shunt size increases. The Potts shunt most substantially lowers the mean pulmonary arterial pressure, from about 105 mmHg to about 75 mmHg. Unlike in the VSD case, the pulmonary arterial pressure with the Potts shunt decreases monotonically with increasing shunt size, but most of the benefit has already occurred with a shunt size of 0.5 cm^2. Our model suggests that there is little benefit in using a larger Potts shunt size than this value. Figure 3 shows the pressures in pulmonary artery and systemic artery for the three interventions, all on the same plot, as functions of the shunt area.
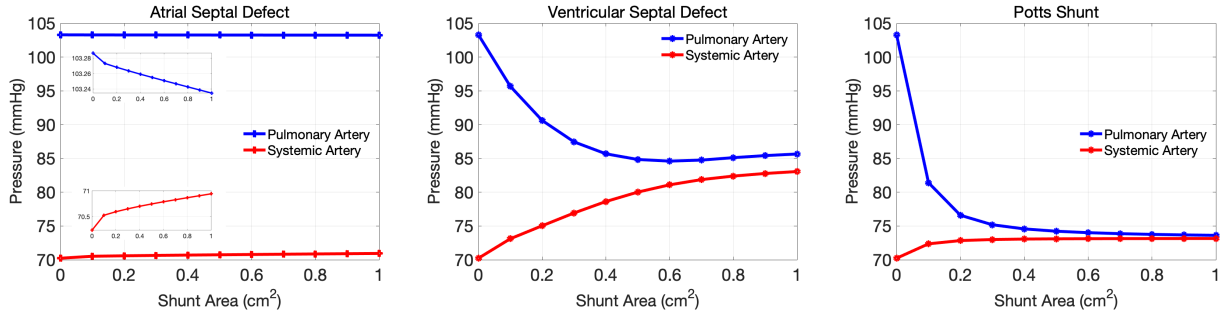

Figure 2: A comparison of pressures in the pulmonary artery (blue) and systemic artery (red) as the shunt area is varied in the ASD, VSD, and Potts shunt. The inset figure shows a zoomed in portion of the results.

We further investigate oxygen transport for each intervention in Figure 4. This figure depicts systemic flow, oxygen saturation, and the rate of oxygen delivery for the three interventions. Systemic flow is relevant here because it is used in the computation of oxygen delivery to the systemic tissues. Oxygen saturation is the oxygen concentration (in mmol/L) expressed as a percentage of 10 mmol/L, which is the maximum possible oxygen concentration in our model. The rate at which oxygen is delivered to the systemic tissues is calculated by multiplying the systemic flow by the systemic arterial oxygen concentration.

All three interventions increase systemic flow. The increase is substantial, however, only in the case of VSD, where the increase in systemic flow has a substantial effect on oxygen delivery to the systemic tissues, as discussed below. All three interventions decrease systemic arterial oxygen saturation. This is inevitable, since the interventions by design are allowing venous blood to bypass the lungs. The effect is smallest in the case of ASD, but since the ASD intervention had essentially no benefit, the fact that it also does the least harm is not really of interest. The VSD and Potts shunt produce similar decreases in systemic arterial oxygen saturation, but these two interventions look quite different from the point of view of oxygen delivery to the systemic tissues. The increase in
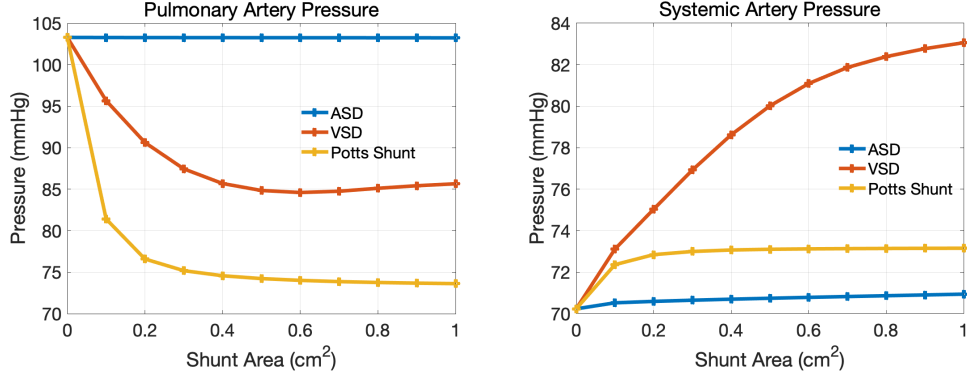
Figure 3: A comparison of pressures in pulmonary artery and systemic artery for the three interventions: the left panel shows the pulmonary artery pressures for the three interventions as the shunt area is varied. The right panel shows the systemic artery pressures for the three interventions as the shunt area is varied. Note different pressure scales in the two panels.

systemic flow in the VSD case seems to compensate nicely for the drop in systemic arterial oxygen saturation. Even at the shunt size of 0.4 cm^2, where the oxygen delivery is the smallest in the VSD case, it is only about 4% smaller than in the pre-intervention state with zero as the shunt size. Recall, however, that the optimal reduction in pulmonary arterial blood pressure occurs in the case of VSD at a shunt size of 0.6 cm^2, and at this shunt size, the reduction of oxygen delivery is even smaller – only about 2.5%.
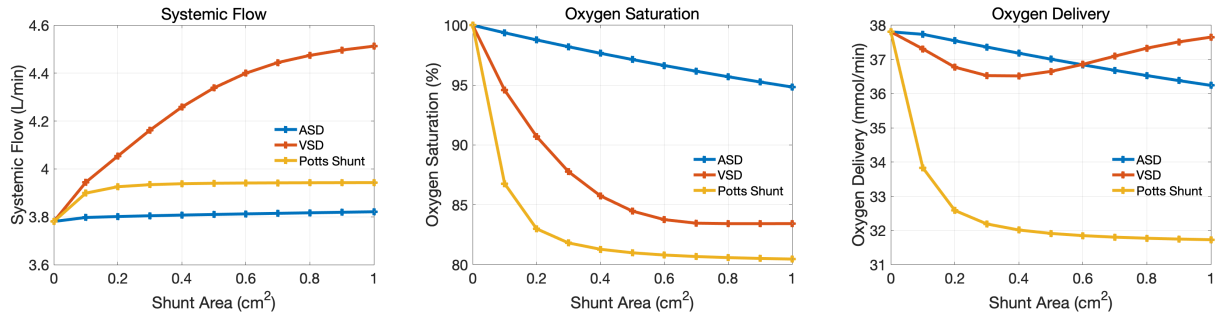

Figure 4: A comparison of systemic flow, oxygen saturation, and oxygen delivery rate for the three interventions: the left panel shows the systemic flow, the middle panel shows the oxygen saturation, and the right panel shows the rate of oxygen delivery to the systemic tissues.

3.2   Shunt flow waveforms

Figures 5, 6, and 7 show waveforms of the shunt flow in each of the three interventions, ASD, VSD, and Potts shunt. Two shunt sizes, 0.1 cm^2 and 1 cm^2, are considered. The last 5 cardiac cycles of a 1000-cycle computer simulation are shown in each case. In all cases, our sign convention is that right-to-left flow is considered positive. Note that the ASD shunt flow is strongly bidirectional, whereas the VSD and Potts shunt flows are exclusively right-to-left. The VSD flow is essentially zero, however, during part of each cardiac cycle, whereas the Potts shunt flow never comes close to zero, but instead is sustained right-to-left flow throughout the cardiac cycle.

Although bidirectional flow does not play an important role in this study, since the ASD intervention does not appear to be useful, it is an important feature of our methodology that it evaluates

11

the shunt flow as a function of time, and not merely the mean flow. This is because bidirectional flow can exchange oxygen between two compartments even when there is no mean shunt flow at all, and this can have a substantial impact on oxygen transport. Indeed, in the congenital heart disease called transposition of the great arteries, the pulmonary and systemic circulations form parallel loops, and there cannot be any mean flow from one to the other. Survival of the patient after birth is then completely dependent on the existence of a bidirectional shunt [24].
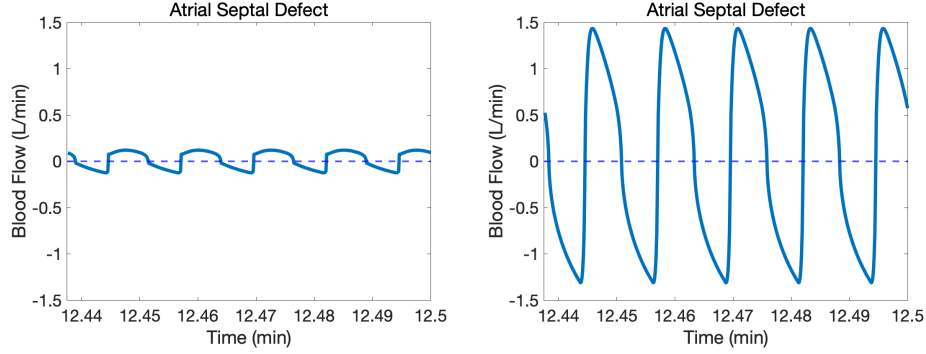

Figure 5: Shunt flow waveforms in the ASD. The left panel shows flow when the shunt area is 0.1 cm^2, and the right panel flow when the shunt area is 1 cm^2.
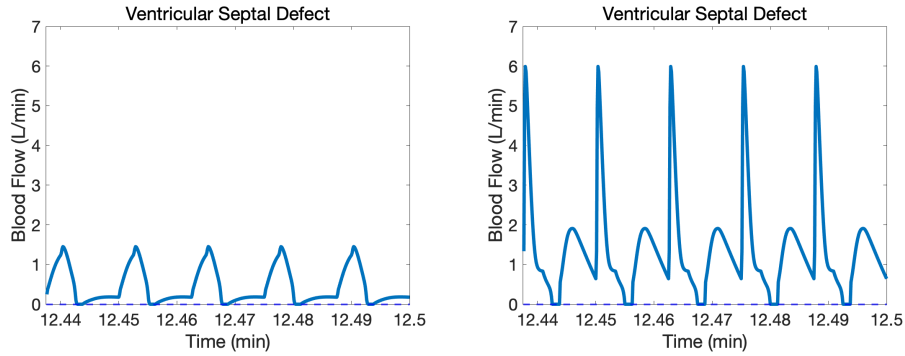

Figure 6: Shunt flow waveforms in the VSD. The left panel shows flow when the shunt area is 0.1 cm^2, and the right panel flow when the shunt area is 1 cm^2.
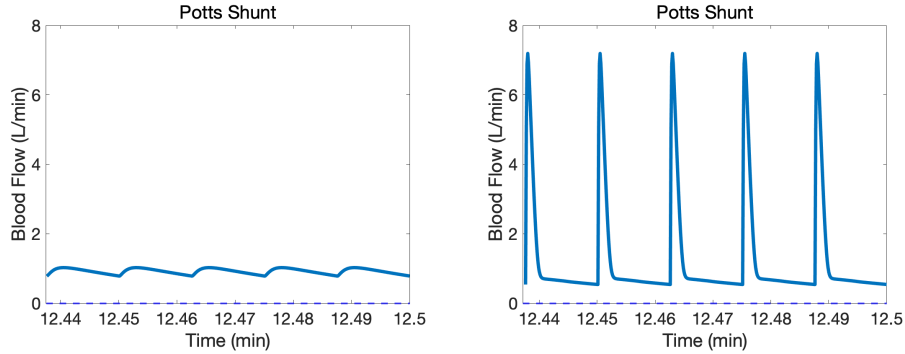

Figure 7: Shunt flow waveforms in the Potts shunt. The left panel shows flow when the shunt area is 0.1 cm^2, and the right panel shows flow when the shunt area is 1 cm^2.

4 Limitations

The specific results reported above may certainly depend upon the specific parameters chosen. In order to apply the methodology of this paper with confidence to any particular patient, it will be necessary to identify the relevant cardiovascular parameters of that patient. Making the model patient-specific is also a way to test the validity of the model, since the pre-operative state of a patient can be used to identify patient-specific parameters, and then the model can be used to predict what the immediately post-operative state of the patient will be. Comparison with the actual post-operative state will then be a strong test of the model. Future work will therefore be directed toward the development of a methodology for identifying the model parameters that correspond best to the state of a particular patient, so that the model can be made useful in clinical practice.

5 Conclusions

In this paper, we have presented a methodology that can be used to study surgical interventions that are designed to alleviate the detrimental effects of refractory pulmonary hypertension. We have illustrated the use of this methodology by comparing three such interventions, all of which are designed to allow some blood flow to bypass the lungs: an atrial septal defect, a ventricular septal defect, and a Potts shunt. For each intervention, we have simulated a range of defect sizes from 0 to 1 cm^2. Our results are that ASD is ineffective at lowering the blood pressure in the pulmonary artery, but that VSD and Potts shunt are both effective, with the greater effect being produced by the Potts shunt. These results are consistent with the fact that an ASD shunt is volume-unloading while a VSD or Potts shunt is pressure-unloading. Both VSD and Potts shunt lower the systemic arterial oxygen saturation in our study, but this is partially compensated by an increase in systemic flow, so that oxygen delivery to the systemic tissues is lowered to a lesser degree than the systemic arterial oxygen saturation. The increase in systemic flow is substantially greater for VSD than for Potts shunt, with the result that oxygen delivery is only slightly reduced in the VSD case, but more substantially reduced in the case of Potts shunt. Thus, when judged by reduction of pulmonary arterial pressure alone, the Potts shunt appears to perform better. When considering oxygen delivery, the VSD appears seems to be the best choice, but it is important to note that this shunt results in blood mixing in the ventricles, and consequently, desaturated blood is delivered to the brain, coronaries arteries, and lower body. In contrast, the Potts shunt results in desaturated blood delivered only to the lower body, since mixing occurs downstream from the carotid arteries; fully saturated blood is delivered to the brain and heart. All of the above effects are quantified in our study as functions of the size of the defect in each case, and this kind of information could be useful to a clinician who needs to decide how large a defect to create.

References

[1] Sebastián Acosta, Charles Puelz, Béatrice Rivière, Daniel J Penny, Ken M Brady, and Craig G Rusin. Cardiovascular mechanics in the early stages of pulmonary hypertension: a computational study. *Biomechanics and Modeling in Mechanobiology*, 16(6):2093–2112, 2017.

[2] Alban-Elouen Baruteau, Emre Belli, Younes Boudjemline, Daniela Laux, Marilyne Lévy, Gérald Simonneau, Adriano Carotti, Marc Humbert, and Damien Bonnet. Palliative Potts shunt for the treatment of children with drug-refractory pulmonary arterial hypertension: updated data

from the first 24 patients. *European Journal of Cardio-Thoracic Surgery*, 47(3):e105–e110, 2015.

[3] D Chemla, Vincent Castelain, P Herve, Y Lecarpentier, and Serge Brimioulle. Haemodynamic evaluation of pulmonary hypertension. *European Respiratory Journal*, 20(5):1314–1331, 2002.

[4] Tammo Delhaas, Yvette Koeken, Heiner Latus, Christian Apitz, and Dietmar Schranz. Potts shunt to be preferred above atrial septostomy in pediatric pulmonary arterial hypertension patients: a modeling study. *Frontiers in Physiology*, 9:1252, 2018.

[5] Christian D Etz, Henryk A Welp, Tony DT Tjan, Andreas Hoffmeier, Ernst Weigang, Hans H Scheld, and Christof Schmid. Medically refractory pulmonary hypertension: treatment with nonpulsatile left ventricular assist devices. *The Annals of Thoracic Surgery*, 83(5):1697–1705, 2007.

[6] Sorin Giusca, Elena Popa, Mihaela Silvia Amzulescu, Ioana Ghiorghiu, Ioan Mircea Coman, Bogdan A Popescu, Marion Delcroix, Jens-Uwe Voigt, Carmen Ginghina, and Ruxandra Jurcut. Is right ventricular remodeling in pulmonary hypertension dependent on etiology? an echocardiographic study. *Echocardiography*, 33(4):546–554, 2016.

[7] Frank C Hoppensteadt and Charles S Peskin. *Modeling and simulation in medicine and the life sciences*. Springer Science & Business Media, 2012.

[8] Gabor Kovacs, Andrea Olschewski, Andrea Berghold, and H Olschewski. Pulmonary vascular resistances during exercise in normal subjects: a systematic review. *European Respiratory Journal*, 39(2):319–328, 2012.

[9] Jane A Leopold. Catheter-based therapies for patients with medication-refractory pulmonary arterial hypertension. *Circulation: Cardiovascular Interventions*, 8(11):e003332, 2015.

[10] Marilyne Levy, David S Celermajer, Elisabeth Bourges-Petit, Maria-Jesus Del Cerro, Fanny Bajolle, and Damien Bonnet. Add-on therapy with subcutaneous treprostinil for refractory pediatric pulmonary hypertension. *The Journal of Pediatrics*, 158(4):584–588, 2011.

[11] Fuyou Liang, Shu Takagi, Ryutaro Himeno, and Hao Liu. Multi-scale modeling of the human cardiovascular system with applications to aortic valvular and arterial stenoses. *Medical and Biological Engineering and Computing*, 47(7):743–755, 2009.

[12] JP Mynard, MR Davidson, DJ Penny, and JJ Smolich. A simple, versatile valve model for use in lumped parameter and one-dimensional cardiovascular models. *International Journal for Numerical Methods in Biomedical Engineering*, 28(6-7):626–641, 2012.

[13] Nasim Naderi. Chapter 11 - Hemodynamic Study. In Majid Maleki, Azin Alizadehasl, and Majid Haghjoo, editors, *Practical Cardiology*, pages 183 – 191. Elsevier, 2018.

[14] Anton Vonk Noordegraaf, Kelly Marie Chin, François Haddad, Paul M Hassoun, Anna R Hemnes, Susan Roberta Hopkins, Steven Mark Kawut, David Langleben, Joost Lumens, and Robert Naeije. Pathophysiology of the right ventricle and of the pulmonary circulation in pulmonary hypertension: an update. *European Respiratory Journal*, 53(1), 2019.

[15] Charles S Peskin and Cheng Tu. Hemodynamics in congenital heart disease. *Computers in Biology and Medicine*, 16(5):331–359, 1986.

[16] M Umar Qureshi, Gareth DA Vaughan, Christopher Sainsbury, Martin Johnson, Charles S Peskin, Mette S Olufsen, and NA Hill. Numerical simulation of blood flow and pressure drop in the pulmonary arterial and venous circulation. *Biomechanics and Modeling in Mechanobiology*, 13(5):1137–1154, 2014.

[17] MK Rausch, A Dam, SERDAR Göktepe, OJ Abilez, and E Kuhl. Computational modeling of growth: systemic and pulmonary hypertension in the heart. *Biomechanics and Modeling in Mechanobiology*, 10(6):799–811, 2011.

[18] Terry Reynolds. The determination of aortic valve area by the gorlin formula: what the cardiac sonographer should know. *Journal of the American Society of Echocardiography*, 3(4):331–335, 1990.

[19] Andrew K Roy, Sean P Gaine, and Kevin P Walsh. Percutaneous atrial septostomy with modified butterfly stent and intracardiac echocardiographic guidance in a patient with syncope and refractory pulmonary arterial hypertension. *Heart, Lung and Circulation*, 22(8):668–671, 2013.

[20] John J Ryan and Stephen L Archer. The right ventricle in pulmonary arterial hypertension: disorders of metabolism, angiogenesis and adrenergic signaling in right ventricular failure. *Circulation Research*, 115(1):176–188, 2014.

[21] Keiko Ryo, Akiko Goda, Tetsuari Onishi, Antonia Delgado-Montero, Bhupendar Tayal, Hunter C Champion, Marc A Simon, Michael A Mathier, Mark T Gladwin, and John Gorcsan III. Characterization of right ventricular remodeling in pulmonary hypertension associated with patient outcomes by 3-dimensional wall motion tracking echocardiography. *Circulation: Cardiovascular Imaging*, 8(6):e003176, 2015.

[22] Nikos Stergiopulos, Jean-Jacques Meister, and Nico Westerhof. Determinants of stroke volume and systolic and diastolic aortic pressure. *American Journal of Physiology-Heart and Circulatory Physiology*, 270(6):H2050–H2059, 1996.

[23] Simone Stickel, Wendy Gin-Sing, Martha Wagenaar, and J Simon R Gibbs. The practical management of fluid retention in adults with right heart failure due to pulmonary arterial hypertension. *European Heart Journal Supplements*, 21(Supplement_K):K46–K53, 2019.

[24] Cheng Tu and Charles S Peskin. Hemodynamics in transposition of the great arteries with comparison to ventricular septal defect. *Computers in Biology and Medicine*, 19(2):95–128, 1989.

[25] Jason Widrich and Mrin Shetty. Physiology, pulmonary vascular resistance. In *StatPearls [Internet]*. StatPearls Publishing, 2020.